Procedia Computer Science

Volume 51, 2015, Pages 795–804

ICCS 2015 International Conference On Computational Science

Surrogate-Based Airfoil Design with Space Mapping and Adjoint Sensitivity

Yonatan A. Tesfahunegn[1*], Slawomir Koziel[1†], Leifur Leifsson[1,2‡], and Adrian Bekasiewicz[1§]

[1] Reykjavik University, Reykjavik, Iceland
[2]Iowa State University, Ames, Iowa, USA
yonatant@ru.is, koziel@ru.is, leifur@iastate.edu, bekasiewicz@ru.is

Abstract

This paper presents a space mapping algorithm for airfoil shape optimization enhanced with adjoint sensitivities. The surrogate-based algorithm utilizes low-cost derivative information obtained through adjoint sensitivities to improve the space mapping matching between a high-fidelity airfoil model, evaluated through expensive CFD simulations, and its fast surrogate. Here, the airfoil surrogate model is constructed though low-fidelity CFD simulations. As a result, the design process can be performed at a low computational cost in terms of the number of high-fidelity CFD simulations. The adjoint sensitivities are also exploited to speed up the surrogate optimization process. Our method is applied to a constrained drag minimization problem in two-dimensional inviscid transonic flow. The problem is solved for several low-fidelity model termination criteria. The results show that when compared with direct gradient-based optimization with adjoint sensitivities, the proposed approach requires 49-78% less computational cost while still obtaining a comparable airfoil design.

Keywords: Aerodynamic shape optimization, surrogate-based modeling, multi-fidelity models, space mapping, adjoint sensitivity.

1 Introduction

Aerodynamic shape optimization (ASO) is important in engineering design (Percival *et al*., 2001; Leoviriyakit *et al*., 2003; Braembussche, 2008; Dumas, 2008; Leifsson *et al*., 2008; Leifsson *et al*., 2013). Modern ASO methodologies (Epstein and Peigin, 2005; Kim *et al*., 2010; Leung *et al*., 2012) use high-fidelity computational fluid dynamic (CFD) simulations as a part of efficient numerical optimization algorithms. However, the use of accurate high-fidelity CFD models in conventional (e.g,

* Engineering Optimization & Modeling Center, School of Science and Engineering
† Engineering Optimization & Modeling Center, School of Science and Engineering
‡ Department of Aerospace Engineering
§ Engineering Optimization & Modeling Center, School of Science and Engineering

Selection and peer-review under responsibility of the Scientific Programme Committee of ICCS 2015

doi:10.1016/j.procs.2015.05.201

gradient-based) optimization techniques leads to a time consuming design process due to the computational expense of the accurate CFD models, and, often, a large design space. In general, the difficulties of the conventional CFD simulation driven optimization can be alleviated to some extent by using adjoint sensitivity information (Jameson, 1988). The advantage of using this technology is that the cost of obtaining the gradients is almost equivalent to one flow solution, irrespective of the number of design variables (Jameson, 1988). The use of adjoints is a necessity for solving large-scale problems. Gradient-based search with adjoint sensitivities is, therefore, the state-of-the-art for solving ASO problems (Kim *et al*., 2001; Martins *et al*., 2005; Mavriplis, 2007). Unfortunately, adjoint sensitivity information is currently not widely available in commercial tools and this limits the use of the approach. However, more and more codes, both commercial codes as well as open source ones, are offering this information and it is expected that it will become standard in the future.

Computationally efficient ASO can also be carried out using surrogate-based optimization (SBO) (Queipo et al., 2005; Forrester and Keane, 2009; Koziel, Echeverria and Leifsson, 2011), particularly if the surrogate model is physics-based (Koziel and Leifsson, 2012), i.e., the surrogate embeds certain knowledge about the high-fidelity CFD model. Physics-based surrogate models rely on the underlying low-fidelity model, which is normally problem specific. The low-fidelity model is a simplified description of the system under consideration. It can be obtained by neglecting certain second-order effects, using simplified equations, or—which is probably the most versatile approach—by exploiting the same CFD solver as used to evaluate the high-fidelity model but with a coarser mesh and/or relaxed convergence criteria (Leifsson and Koziel, 2011).

Several SBO algorithms exploiting physical surrogates have been reported in the literature (Alexandrov and Lewis, 2001; Bandler *et al*., 2004; Echeverria and Hemker, 2005; Koziel *et al*., 2008; Koziel, 2010) and one of them is space mapping (SM), which was originally developed for simulation-driven design in microwave engineering (Bandler *et al*., 2004), and for aerodynamic shape optimization (Koziel and Leifsson, 2012).

Recently, a methodology for combining SM and adjoint sensitivities for simulation-driven design in microwave engineering was proposed (Koziel *et al*., 2012; Koziel *et al*. 2013). A similar approach is developed in this work for ASO with the purpose of speeding up surrogate-based optimization of CFD-simulated models using space mapping. In our approach, adjoint sensitivity of both high- and low-fidelity model is utilized to improve the prediction power of the SM surrogate model, whereas the low-fidelity sensitivity data allows for accelerating the surrogate model optimization process. The proposed algorithm is applied to a benchmark problem involving transonic airfoil shape optimization and compared with the results obtained by means the conventional approach, i.e., direct high-fidelity model optimization (also with adjoint sensitivities). The results indicate that SM with adjoint sensitivities can provide a significant speed-up of the design process when compared to the direct method.

2 Problem Statement

In general, achieving an optimum aerodynamic performance (e.g., minimum drag for a given lift) is the key challenge in airfoil shape optimization. We formulate the problem as a constrained nonlinear minimization task, i.e., for a given operating condition, solve

$$\begin{aligned} &\min_{\mathbf{x}} f(\mathbf{x}) \\ &s.t.\ g_j(\mathbf{x}) \le 0,\ j = 1,\ldots,M \\ &\quad h_k(\mathbf{x}) = 0,\ k = 1,\ldots,N \\ &\quad \mathbf{l} \le \mathbf{x} \le \mathbf{u} \end{aligned} \quad , \tag{1}$$

where $f(\mathbf{x})$ is the objective function, $\mathbf{x}$ is the design variable vector, $g_j(\mathbf{x})$ are the inequality constraints, M is the number of the inequality constraints, $h_k(\mathbf{x})$ are the equality constraints, N is the number of the equality constraints, and $\mathbf{l}$ and $\mathbf{u}$ are the design variables lower and upper bounds, respectively.

In this work, we consider drag minimization with the following formulation. For a given operating condition of a Mach number M_∞ and an angle of attack α, minimize the drag coefficient, $f(\mathbf{x}) = C_d(\mathbf{x})$, subject to constraints on the section lift coefficient, $g_1(\mathbf{x}) = C_{l.min} - C_l(\mathbf{x}) \le 0$, and the cross-sectional area, $g_2(\mathbf{x}) = t_{min} - t(\mathbf{x}) \le 0$, where C_l is the section lift coefficient, $C_{l.min}$ is a target section lift coefficient, t is the airfoil thickness as a function of chord, and t_{min} is a minimum thickness. It is assumed that the aerodynamic characteristics (f, and g_i) are obtained by a computationally expensive model. In particular, a high-fidelity CFD model is employed in this work for evaluating the aerodynamic characteristics.

3 Adjoint Enhanced Space Mapping Optimization

In this section, we describe in detail the proposed optimization procedure, in particular, the space mapping algorithm, and the construction of the space mapping surrogate model and its enhancement based on adjoint sensitivity information obtained from the Stanford University Unstructured (SU2) open source CFD solver (Palacios *et al*., 2013). We also formulate an adjoint-based algorithm for fast optimization of the surrogate model.

3.1 Space Mapping Algorithm

A generic space mapping algorithm produces a sequence $\boldsymbol{x}^{(i)}$, $i = 0, 1, \ldots$, of approximate solutions to (1) (here, $\boldsymbol{x}^{(0)}$ is the initial design) as

$$\mathbf{x}^{(i+1)} = \arg \min_{\mathbf{x}, \|\mathbf{x}-\mathbf{x}^{(i)}\| \le \delta^{(i)}} H(s^{(i)}(\mathbf{x})), \tag{2}$$

where $s^{(i)}(\boldsymbol{x}) = [C_{l.s}{}^{(i)}(\boldsymbol{x})\ C_{d.s}{}^{(i)}(\boldsymbol{x})\ A_s{}^{(i)}(\boldsymbol{x})]^T$ is a surrogate model at iteration i and $\boldsymbol{x}^{(i)}$, $i = 0, 1, \ldots$, is the sequence of approximate solutions to (1). Assuming that the surrogate model embeds certain knowledge about the system of interest, its generalization capability is substantially better than that of, e.g., simple linear expansion models such as first- or second-order Taylor ones. Consequently, the number of iterations of (2) necessary to converge to an optimum design is usually very small (say, a few). This, in conjunction with the fact that the surrogate model update in each iteration requires only one new high-fidelity model evaluation (at the design produced at the previous iteration), permits considerable reduction of the overall optimization cost compared to most conventional methods.

The surrogate model optimization is embedded in the trust-region framework (Conn, *et al.*, 2000), which is used here as a convergence safeguard. More specifically, the surrogate optimization is restricted to the vicinity of the current design $\mathbf{x}^{(i)}$ of the size $\delta^{(i)}$. The trust region radius is updated in each iteration based on the so-called gain ratio, which is the ratio of the actual improvement of the high-fidelity objective function versus the one predicted by the surrogate model.

The surrogate model is a composition of the low-fidelity model and simple, usually linear,

transformations (or mappings) (Koziel, Chang, and Bandler, 2006). In this work, we use output space mapping (Koziel and Leifsson, 2012) enhanced by sensitivity information from both the high- and the low-fidelity models.

3.2 Surrogate Model Construction Using Output Space Mapping and Adjoint Sensitivities

The space mapping surrogate model utilized in this work takes the form of

$$s^{(i)}(\mathbf{x}) = \mathbf{A}^{(i)} \circ c(\mathbf{x}) + \mathbf{D}^{(i)} + \mathbf{q}^{(i)} + \mathbf{E}^{(i)} \cdot (\mathbf{x} - \mathbf{x}^{(i)}), \tag{3}$$

Here, the multiplicative and additive response correction is defined, at the component level as

$$\mathbf{A}^{(i)} \circ c(\mathbf{x}) + \mathbf{D}^{(i)} + \mathbf{q}^{(i)} = \left[a_l^{(i)} C_{l.c}(\mathbf{x}) + d_l^{(i)} + q_l^{(i)} \quad a_d^{(i)} C_{d.c}(\mathbf{x}) + d_d^{(i)} + q_d^{(i)} \quad A_c^{(i)}(\mathbf{x}) \right]^T, \tag{4}$$

where ° denotes component-wise multiplication. Note that there is no need to map A_c because $A_c(\boldsymbol{x}) = A_f(\boldsymbol{x})$ for all $\boldsymbol{x}$.

The matrix $\mathbf{E}^{(i)}$ in the linear part of the correction (3) is defined as

$$\mathbf{E}^{(i)} = \begin{bmatrix} [\nabla C_{l.f}(\mathbf{x}^{(i)}) - a_l^{(i)} \nabla C_{l.c}(\mathbf{x}^{(i)})]^T \\ [\nabla C_{d.f}(\mathbf{x}^{(i)}) - a_d^{(i)} \nabla C_{d.c}(\mathbf{x}^{(i)})]^T \\ 0 \end{bmatrix}, \tag{5}$$

The response correction parameters $\mathbf{A}^{(i)}$ and $\mathbf{D}^{(i)}$ are obtained by solving

$$\left[\mathbf{A}^{(i)}, \mathbf{D}^{(i)} \right] = \arg\min_{[\mathbf{A},\mathbf{D}]} \sum_{k=0}^{i} \left\| f(\mathbf{x}^{(k)}) - \mathbf{A} \circ c(\mathbf{x}^{(k)}) + \mathbf{D} \right\|^2, \tag{6}$$

i.e., the response scaling is supposed to (globally) improve the matching for all previous iteration points. The additive response correction term $\mathbf{q}^{(i)}$ is defined as

$$\mathbf{q}^{(i)} = f(\mathbf{x}^{(i)}) - \left[\mathbf{A}^{(i)} \circ c(\mathbf{x}^{(i)}) + \mathbf{D}^{(i)} \right], \tag{7}$$

i.e., it ensures perfect matching between the surrogate and the high-fidelity model at the current design $\boldsymbol{x}^{(i)}$, $s^{(i)}(\boldsymbol{x}^{(i)}) = f(\boldsymbol{x}^{(i)})$ (so-called zero-order consistency).

Both $\boldsymbol{A}^{(i)}$, $\boldsymbol{D}^{(i)}$ and $\boldsymbol{q}^{(i)}$ can be calculated analytically so that there is no need to carry out nonlinear-minimization. Terms $\boldsymbol{A}^{(i)}$ and $\boldsymbol{D}^{(i)}$ can be obtained as

$$\begin{bmatrix} a_l^{(i)} \\ d_l^{(i)} \end{bmatrix} = (\mathbf{C}_l^T \mathbf{C}_l)^{-1} \mathbf{C}_l^T \mathbf{F}_l, \qquad \begin{bmatrix} a_d^{(i)} \\ d_d^{(i)} \end{bmatrix} = (\mathbf{C}_d^T \mathbf{C}_d)^{-1} \mathbf{C}_d^T \mathbf{F}_d, \tag{8}$$

where

$$\mathbf{C}_l = \begin{bmatrix} C_{l.c}(\mathbf{x}^{(0)}) & C_{l.c}(\mathbf{x}^{(1)}) & \cdots & C_{l.c}(\mathbf{x}^{(i)}) \\ 1 & 1 & \cdots & 1 \end{bmatrix}^T, \tag{9}$$

$$\mathbf{F}_l = \left[C_{l.f}(\mathbf{x}^{(0)}) \quad C_{l.c}(\mathbf{x}^{(1)}) \quad \cdots \quad C_{l.f}(\mathbf{x}^{(i)}) \right]^T, \tag{10}$$

$$\mathbf{C}_d = \begin{bmatrix} C_{d.c}(\mathbf{x}^{(0)}) & C_{d.c}(\mathbf{x}^{(1)}) & \cdots & C_{d.c}(\mathbf{x}^{(i)}) \\ 1 & 1 & \cdots & 1 \end{bmatrix}^T, \tag{11}$$

$$\mathbf{F}_d = \left[C_{d.f}(\mathbf{x}^{(0)}) \quad C_{d.c}(\mathbf{x}^{(1)}) \quad \cdots \quad C_{d.f}(\mathbf{x}^{(i)}) \right]^T, \tag{12}$$

which is a least-square optimal solution to the linear regression problem $\boldsymbol{C}_l a_l^{(i)} + d_l^{(i)} = \boldsymbol{F}_l$ and $\boldsymbol{C}_d a_d^{(i)} + d_d^{(i)} = \boldsymbol{F}_d$, equivalent to (6). Note that the matrices $\boldsymbol{C}_l^T \boldsymbol{C}_l$ and $\boldsymbol{C}_d^T \boldsymbol{C}_d$ are non-singular for $i > 1$. For $i = 1$ only the multiplicative correction with $\boldsymbol{A}^{(i)}$ components are used, which can be calculated in a similar way.

The linear term $\mathbf{E}^{(i)} \cdot (\mathbf{x} - \mathbf{x}^{(i)})$ in (3), defined as in (5) ensures first-order consistency between the surrogate and the high-fidelity model, that is, perfect agreement of the model gradients, both for the drag and the lift coefficient. While this requires derivative information, in our approach, it is obtained at only small computational overhead using adjoint sensitivities. Satisfaction of both zero- and first-order consistency ensures (provided that the functions involved are sufficiently smooth; Alexandrov and Lewis, 2001) convergence of the iterative process (2) to at least local optimum of the original problem (1).

3.3 Fast Adjoint-Based Surrogate Optimization

Adjoint sensitivity is also utilized to speed up the surrogate model optimization process (2). More specifically, in order to obtain the design $\mathbf{x}^{(i+1)}$, the following trust-region-based process is launched

$$\mathbf{x}^{(i+1.k+1)} = \arg \min_{\mathbf{x}, \|\mathbf{x} - \mathbf{x}^{(i+1.k)}\| \le \delta^{(i.k)}} H(L^{(i.k)}(\mathbf{x})), \tag{13}$$

where $\mathbf{x}^{(i+1.k)}$, $k = 0, 1, \ldots$, is the sequence approximating $\mathbf{x}^{(i+1)}$, with $\mathbf{x}^{(i+1.0)} = \mathbf{x}^{(i)}$; $L^{(i.k)}$ is the linear approximation of the surrogate model $s^{(i)}$, established at $\mathbf{x}^{(i+1.k)}$ of the form

$$L^{(i.k)}(\mathbf{x}) = s^{(i)}(\mathbf{x}^{(i+1.k)}) + \nabla s^{(i)}(\mathbf{x}^{(i+1.k)}) \cdot (\mathbf{x} - \mathbf{x}^{(i+1.k)}), \tag{14}$$

Here, the gradient of $s^{(i)}$ is calculated using adjoint sensitivity data of the low-fidelity model c. $\delta^{(i.k)}$ is the trust region radius of the inner optimization loop, updated independently from the trust region radius $\delta^{(i)}$ in (2).

Because of using adjoint data, the number of iterations (therefore, the number of low-fidelity model evaluations) while solving (2) through (14) is low, which allows to greatly reduce the overall cost of the optimization process.

4 Transonic Airfoil Design Applications

We apply the proposed algorithm to the design of transonic airfoils. This section provides a description of the problem setup, design variables, CFD models, and results of numerical optimization studies.

4.1 Problem Description

The objective is to minimize the drag coefficient (C_d) of a modified NACA 0012 airfoil section at a free-stream Mach number of M_∞ = 0.85 and an angle of attack α = 0 deg., subject to a minimum thickness constraint. The optimization problem is stated as

$$\min_{\mathbf{l}\le\mathbf{x}\le\mathbf{u}} C_d\,, \tag{15}$$

where **x** is the vector of design variables, and **l** and **u** are the lower and upper bounds, respectively. The thickness constraint is stated as

$$z(x) \ge z(x)_{baseline}\,, \tag{16}$$

where $z(x)$ is the airfoil thickness, $x \in [0,1]$ is the chord-wise location, and $z(x)_{baseline}$ is the thickness of the baseline airfoil, which is a modified version of the NACA 0012, defined as

$$z(x)_{baseline} = \pm 0.6\left(0.2969\sqrt{x} - 0.1260x - 0.3516x^2 + 0.2843x^3 - 0.1036x^4\right). \tag{17}$$

4.2 Formulation and Algorithm Setup

The problem is formulated as described in Sections 2 and 3. It is solved using the adjoint-enhanced space mapping (AESM) algorithm in Section 3. The CFD models are explained in Sections 4.4 and 4.5.

In the original AESM (Koziel *et al*., 2012) the maximum number of low-fidelity model evaluations was set to 5 during the surrogate optimization processes. In this work, in order to investigate the performance of the algorithm, we set three different maximum number of low-fidelity model evaluations, i.e., 10, 15 and unlimited number (terminated upon convergence) with the following acronyms AESM10, AESM15 and AESM∞, respectively. The results of the numerical experiments will be compared with the high-fidelity model directly optimized using a gradient-based algorithm with adjoint sensitivity (Tesfahunegn *et al.*, 2015).

4.3 Design Variables

We use the Hicks-Henne bump functions (Hicks and Henne, 1978) as the design variables. In this approach a baseline airfoil shape, $z(x)_{baseline}$, is deformed to yield a new airfoil shape, $z(x)$. The new airfoil shape can be written as

$$z(x) = z(x)_{baseline} + \Delta z(x)\,, \tag{18}$$

where

$$\Delta z(x) = \sum_{n=1}^{N} \delta_n f_n(x) \tag{19}$$

is the total deformation with

$$f_n(x) = \sin^3\left(\pi\, x^{e_n}\right) \tag{20}$$

being the Hicks-Henne bump functions, δ_n is the deformation amplitude, N is the number of deformations, and

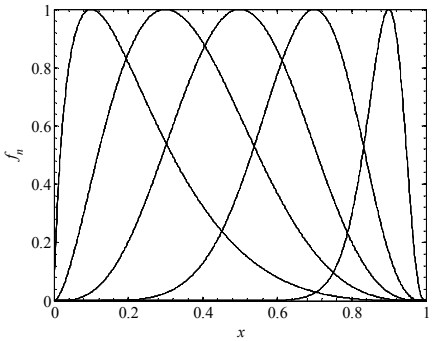

Figure 1: Hicks-Henne bump functions with maxima at x_n = 0.1, 0.3, 0.5 0.7, and 0.9, b = 3.0, and δ = 1.0. where $x_n \in [0,1]$ is the location of the function maximum.

$$e_n = \frac{\log_{10}(0.5)}{\log_{10}(x_n)} \ . \tag{21}$$

Examples of a few Hicks-Henne bump function shapes are shown in Figure 1. In airfoil shape optimization, the number of bumps, N, and their locations of maxima, x_n, are, typically, fixed. The designable parameters are then the amplitudes, δ_n, with the design variable vector written as $\mathbf{x} = [\delta_1\ \delta_2\ \cdots\ \delta_N]^T$. In our application example, we use N = 15 with the bumps equally spaced in $x_n \in [0.05,0.95]$.

4.4 High-Fidelity CFD Model

Two-dimensional transonic flow past airfoil sections is considered. The flow is assumed to be steady, inviscid, and adiabatic, with no body forces. The compressible Euler equations are taken as the governing fluid flow equations.

The high-fidelity model is employs the Stanford University Unstructured (SU2) (Palacios *et al*., 2013) computer code for fluid flow simulations. In particular, an implicit density-based formulation is used and the inviscid fluxes are calculated by an upwind-biased second-order spatially accurate Roe flux scheme. Asymptotic convergence to a steady state solution is obtained in each case. The solution convergence criterion for the high-fidelity model is the one that occurs first of the following: a reduction in all the residuals by six orders, or a maximum number of iterations of 1,000.

The high-fidelity model grids used in this study are hyperbolic C-mesh (Kinsey and Barth, 1984). The farfield is set 100 chords away from the airfoil surface. The grids have 630 points in the streamwise direction and 360 points in the direction normal to the airfoil surface. The region behind the airfoil to the farfield contains 360 points. The grid points were clustered at the trailing edge and the leading edge of the airfoil to give a minimum streamwise spacing of 0.001 × chord length. The distance from the airfoil surface to the first node is $5{\cdot}10^{-4}$ × chord length. The mesh has roughly 163,000 cells. A typical evaluation time of the high-fidelity model is around 27 minutes. Example grid is shown in Figure 2.

4.5 Low-Fidelity CFD Model

The low-fidelity model is based on the same CFD model as the high-fidelity one but reduced levels of discretization as well as a relaxed flow solver convergence criteria. In particular, it has a 140 × 80 grid with about 8,000 cells. The maximum number of flow solver iterations is set to 400. Typical evaluation time is 1 minute. The average high-to-low simulation time ratio is approximately 25.

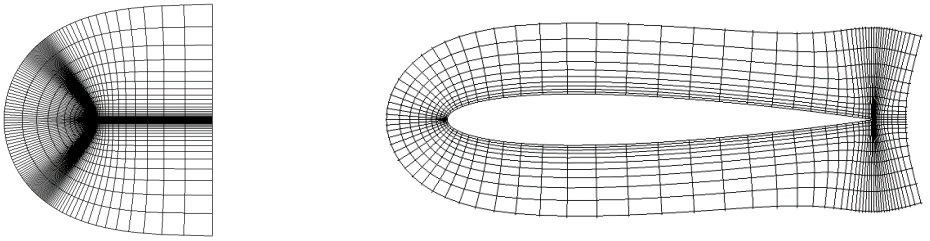

Figure 2: A hyperbolic C-grid showing a farfield view (left) and a view close to the surface (right).

4.6 Results

The numerical results are shown in Table 1. The problem is described in Section 1. The initial and optimized airfoil shapes are shown in Figure 3(a), and their corresponding pressure coefficient distributions are shown in Figure 3(b). In Table 1, the acronyms AESM10, AESM15 and AESM∞ refer to AESM with different numbers of the low-fidelity model evaluations per design iteration as described in Section 4.2.

We can see that both the direct optimization and the AESM algorithm obtain comparable airfoil shapes, with the direct shape being in between the AESM designs, but thicker in the aft (Figure 3(a)). The lift coefficient is close to zero in all cases except AESM10, while the direct design has 139 d.c. (1 drag count = 10^{-4}) and the AESM10, AESM15 and AESM∞ designs 144, 157, and 161 d.c., respectively, with a difference of 5, 18, and 22 d.c, respectively. The shock strength is similar for all cases, as can be seen from Figure 3(b), but the shock locations are slightly different, causing the differences in the drag. In terms of computational cost, the direct approach needs 49 high-fidelity model evaluations, whereas AESM10 needs 77 evaluations of low fidelity-model and 7 high-fidelity model, AESM15 requires 179 and 17 and AESM∞ needs 113 and 8 – yielding a total cost of less than 11, 25, and 13 equivalent high-fidelity evaluations, respectively, which are 38 (about 77 %), 24 (about 49 %) and 36 (about 74 %) evaluations fewer than the direct approach. It can be concluded from these results that the number of low-fidelity model evaluations set for the surrogate model has a significant impact on both the total cost as well as the drag coefficient value.

Table 1. Numerical results for drag minimization of the modified NACA 0012

Variable	Drag minimization $M_\infty = 0.85$, $\alpha = 0°$				
	Initial	Direct[#]	AESM10[&]	AESM15[&]	AESM∞[&]
C_l	0.0000	0.0092	0.0408	0.0020	-0.0038
C_d	0.0471	0.0139	0.0144	0.0157	0.0161
A	0.0817	0.0989	0.0998	0.0978	0.0978
N_c	-	-	77	179	113
N_f	-	49	7	17	8
Cost[*]	–	49	< 11	< 25	< 13

[#] Design obtained through Direct optimization of the high-fidelity model using the gradient-based algorithm with adjoint sensitivity.

[&] Design obtained using the adjoint enhanced space mapping optimization algorithm by varying the maximum number of low-fidelity model evaluations as described in Section 4.2.

[*] The total optimization cost is expressed in terms of the equivalent number of high-fidelity model evaluations. The ratio of high-to-coarse simulation time is 25.

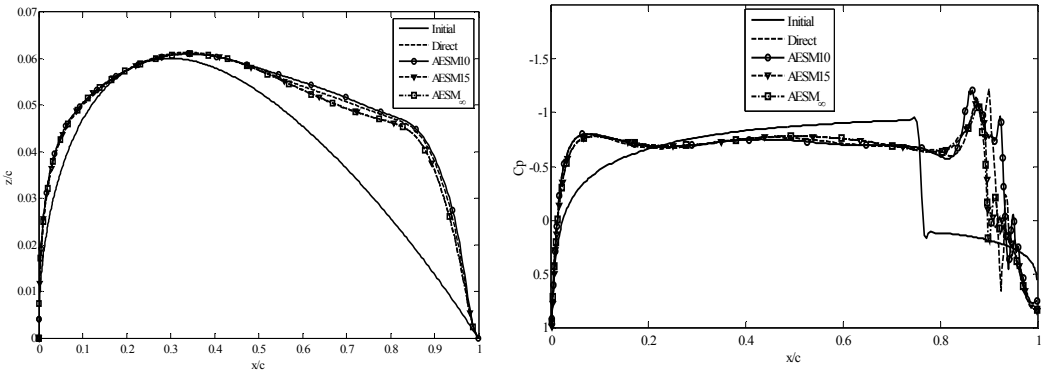

Figure 3: Optimization results: (a) the initial and optimized airfoil shapes, and (b) the pressure coefficient distributions for the initial and optimized designs.

5 Conclusion

A robust and computationally efficient optimization methodology for the design of transonic airfoil is presented. Our approach exploits a low-fidelity CFD model and adjoint-enhanced space mapping technique to create fast and reliable surrogate model that is subsequently used to yield approximate optimum design of the expensive, high fidelity model at low cost. The numerical results show that significant savings are possible when the proposed algorithm is compared to the direct high-fidelity model optimization. In future work, we will investigate in more detail the effects of the surrogate model optimization termination criteria. Moreover, we will investigate the properties of the algorithm in terms of its robustness and scalability to problems of three dimensions (such as wings, and wing-body cases).

References

Alexandrov, N.M., Lewis, R.M., Gumbert, C.R., Green, L.L., and Newman, P.A. (2000) *Optimization with Variable-Fidelity Models Applied to Wing Design.* 38th Aerospace Sciences Meeting & Exhibit, Reno, NV, AIAA Paper 2000-0841.

Alexandrov, N.M. and Lewis, R.M. (2001) *An overview of first-order model management for engineering optimization*, Optimization and Engineering, vol. 2, no. 4, pp. 413-430.

Braembussche, R.A., (2008) *Numerical Optimization for Advanced Turbomachinery Design.* In *Optimization and Computational Fluid Dynamics*, Thevenin, D., Janiga, G. (Eds.), Springer, pp. 147-189.

Bandler, J.W., Cheng, Q.S., Dakroury, S.A.,Mohamed, A.S., Bakr, M.H., Madsen K., and Sondergaard,J. (2004) *Space mapping: the state of the art*, IEEE Trans. Microwave Theory Tech., vol. 52, no. 1, pp. 337-361.

Bandler, J.W., Koziel S., and Madsen K. (2006) *Space mapping for engineering optimization*, SIAG/Optimization Views-and-News Special Issue on Surrogate/Derivative-free Optimization, vol. 17, no. 1, pp. 19-26.

Conn, A.R., Gould, N.I.M., Toint, P.L. (2000) Trust Region Methods. MPS-SIAM Series on Optimization.

Dumas, L., (2008) *CFD-based Optimization for Automotive Aerodynamics*, In Optimization and Computational Fluid Dynamics, Thevenin, D. and Janiga, G., Editors, Springer, pp. 191-214.

Echeverria, D., and Hemker, P.W. (2005) *Space mapping and defect correction*, CMAM Int. Mathematical Journal Computational Methods in Applied Mathematics*, vol.* 5, pp. 107-136.

Epstein, B., and Peigin, S. (2005) *Constrained Aerodynamic Optimization of Three-Dimensional Wings Driven by Navier-Stokes Computations*, AIAA Journal, Vol. 43, No. 9 , pp. 1946-1957.

Forrester, A.I.J., and Keane, A.J. (2009) *Recent advances in surrogate-based optimization.* Prog. in Aerospace

Sciences, vol. 45, no. 1-3, pp. 50-79.

Hicks, R.M., and Henne, P.A. (1978) *Wing Design by Numerical Optimization.* Journal of Aircraft, Vol. 15, No. 7, pp. 407-412.

Jameson, A., (1988) *Aerodynamic Design via Control Theory.* Journal of Scientific Computing, Vol. 3, pp. 233-260.

Koziel, S., Cheng Q.S, and Bandler J.W. (2008) *Space mapping*, IEEE Microwave Magazine, vol. 9, no. 6, pp. 105-122.

Koziel, S. (2010) *Shape*-preserving response prediction for microwave design optimization, IEEE *Trans. Microwave Theory and Tech.*, vol. 58, no. 11, pp. 2829-2837.

Koziel, S., Echeverría-Ciaurri, D., and Leifsson, L. (2011) *Surrogate-based methods.* In S. Koziel and X.S. Yang (Eds.) *Computational Optimization, Methods and Algorithms*, Series: Studies in Computational Intelligence, Springer-Verlag, pp. 33-60.

Koziel, S., Ogurstov S., Bandler, J.W., Cheng, Q.S. (2012) *Robust Space Mapping Optimization Exploiting EM-Based Models with Adjoint Sensitivities,* Microwave Symposium Digest (MTT), IEEE MTT-S International, Montreal, QC, June 17-22.

Koziel, S. and Leifsson, L., (2012) *Knowledge-Based Airfoil Shape Optimization Using Space Mapping. 30th* AIAA Applied Aerodynamics Conference, New Orleans, Louisiana, June 25-28.

Koziel, S., and Leifsson, L. (2013) *Surrogate-Based Aerodynamic Shape Optimization by Variable-Resolution Models.* AIAA Journal, vol. 51, no. 1, pp. 94–106.

Koziel, S., Leifsson, L., and Ogurtsov, S. (2013) *Reliable EM-driven microwave design optimization using manifold mapping and adjoint sensitivity.* Microwave and Optical Technology Letters, vol. 55, no. 4, 2013, pp. 809-813.

Kim, S., Hosseini, K., Leoviriyakit, K., and Jameson, A. (2010) *Enhancement of Class of Adjoint Design Methods via Optimization of Parameter*, AIAA Journal, Vol. 48, No. 6, pp. 1072-1076.

Kim, H., Obayashi, S., and Nakahashi, K. (2001) *Aerodynamic optimization of supersonic transport wing using unstructured adjoint method*, AIAA Journal, Vol. 39, pp. 1011-1020

Leifsson, L., Ko, A., Mason, W., Schetz, J., Grossman, B., and Haftka, R. (2013) *Multidisciplinary Design Optimization of Blended-Wing-Body Transport Aircraft with Distributed Propulsion*. Aerospace Science and Technology, vol. 25, Issue 1, 2013, pp. 16-28.

Leifsson, L., Saevarsdottir, H., Sigurdsson, S., and Vesteinsson, A. (2008) *Grey-Box Modeling of an Ocean Vessel for Operational Optimization.* Simulation Modelling Practice and Theory, vol. 16, no. 8, 2008, pp. 923-932.

Lepine, J., Guibault, F., Trepanier, J.-Y., and Pepin, F. (2001) *Optimized Nonuniform Rational B-Spline Geometrical Representation for Aerodynamic Design of Wings*. AIAA Journal, Vol. 39, No. 11, pp. 2033-2041.

Leoviriyakit, K., Kim, S., and Jameson, A. (2003) *Viscous Aerodynamic Shape Optimization of Wings including Planform Variables.* 21st Applied Aerodynamics Conference, Orlando, Florida, June 23-26.

Leung, T.M., and Zingg, D.W. (2012) *Aerodynamic Shape Optimization of Wings Using a Parallel Newton-Krylov Approach*, AIAA Journal, Vol. 50, No. 3 , pp. 540-550.

Mason, W.H., (1990) *Analytic Models for Technology Integration in Aircraft Design.* AIAA-90-3262.

Martins, J.R.R.A, Alonso, J.J., and Reuther, J.J. (2005) *A coupled-adjoint sensitivity analysis method for high-fidelity aero-structural design*, Optimization and Engineering, 6, pp. 33-62.

Mavriplis, D. J. (2007) *Discrete Adjoint-Based Approach for Optimization Problems on Three-Dimensional Unstructured Meshes*, AIAA Journal, Vol. 45, No. 4.

Percival, S., Hendrix, D., and Noblesse, F. (2001) *Hydrodynamic Optimization of Ship Hull Forms*, Applied Ocean Research, Vol. 23, No. 6, pp. 337-355.

Palacios, F., Colonno, M. R., Aranake, A. C., Campos, A., Copeland, S. R., Economon, T. D., Lonkar, A. K., Lukaczyk, T. W., Taylor, T. W. R., and Alonso, J. J. (2013) *Stanford University Unstructured (SU^2): An open-source integrated computational environment for multi-physics simulation and design*, AIAA Paper 2013-0287, 51st AIAA Aerospace Sciences Meeting and Exhibit, Grapevine, Texas, USA,

Queipo, N.V, Haftka, R.T., Shyy, W., Goel, T.,Vaidynathan, R. and Tucker, P.K. (2005) *Surrogate-based analysis and optimization*, Progress in Aerospace Sciences, vol. 41, no. 1, pp. 1-28.

Robinson, T.D., Eldred, M.S., Willcox, K.E., and Haimes, R. (2008) *Surrogate-Based Optimization Using Multifidelity Models with Variable Parameterization and Corrected Space Mapping.* AIAA Journal, vol. 46, no. 11.

Tesfahunegn, Y.A., Koziel, S., and Leifsson, L. (2015) *Surrogate-Based Airfoil Design with Multi-Level Optimization and Adjoint Sensitivity*, 53rd AIAA Aerospace Sciences Meeting, Kissimmee, Florida, January 5-9.